IEEE Access
Multidisciplinary | Rapid Review | Open Access Journal

Received September 13, 2020, accepted September 26, 2020, date of publication September 30, 2020,
date of current version October 9, 2020.

Digital Object Identifier 10.1109/ACCESS.2020.3027834

Transformer Condition Monitoring Based on Load-Varied Vibration Response and GRU Neural Networks

KAIXING HONG[1], JIE PAN[2], (Member, IEEE), AND MING JIN[2]
[1]College of Mechanical and Electrical Engineering, China Jiliang University, Hangzhou 310018, China
[2]Department of Mechanical Engineering, The University of Western Australia, Perth, WA 6009, Australia

Corresponding author: Kaixing Hong (hongkaixing@cjlu.edu.cn)

This work was supported in part by the National Natural Science Foundation of China under Grant 51805504, and in part by the Natural Science Foundation of Zhejiang Province under Grant LQ18F030008.

ABSTRACT Study of the vibration mechanisms of transformer windings may lead to useful applications of vibration techniques to transformer online diagnosis. In a power transformer, the clamping force provides a boundary mechanical constraint to ensure the integrity of the winding. Thus, the looseness of the clamping force is an important health indicator for a transformer. Although the effect of clamping force on a winding's stiffness and natural frequencies is known, the effect of time-varying load current on these natural frequencies remains unsolved. In this paper, this effect is investigated by studying the mechanical frequency response function of an on-load single-phase winding under different clamping forces and variation of the harmonic amplitude of in-service transformers with load current. Then, a gated recurrent unit (GRU) neural network is used to explore the relationship between current sequence and vibration sequence for operating transformers. This study shows that the electromagnetic force induced by the load current affects the vibration response of the winding structure, especially when the looseness of the clamping force is significant. A potential application of the observed phenomenon for online detection of winding conditions is also illustrated.

INDEX TERMS Dynamic winding model, gated recurrent unit, natural frequency change, transformer vibration.

I. INTRODUCTION

Power transformers are important devices for electrical energy conversion and transmission. Their health status is related to the reliability of electric distribution systems. In recent years, many techniques have been developed to determine the condition of transformers, including frequency response analysis, short-circuit impedance measurement, and dissolved gas analysis [1], [2]. The winding structure is more prone to the risk of damage due to an overload current impulse, and its condition is critical to a transformer's operational lifetime [3]. The winding clamping pressure is an important factor affecting the short-circuit strength of a power transformer [4]. Increased concerns about fault detection and diagnosis efficiency in a smart-grid context have motivated research into developing online non-intrusive monitoring techniques [5]. Previous studies have shown that transformer vibration is connected with the mechanical properties of windings, and the vibration technique has been used to provide diagnostic information [6]–[9].

The mathematical model of transformer windings, known as the static winding model, has been well studied in past decades. In the 1970s, Swihart *et al.* used a multiple lumped spring-mass system to represent the axial vibration of transformer windings, and investigated the dynamic stress-strain characteristics of insulations in detail [10]. With the development of computer technologies, finite-element models were used to obtain a more accurate and intuitive result [11]. In the static winding model, the structural parameters of the windings are independent of load, which can be obtained by the free vibration test. Geng *et al.* extracted the modal parameters of windings from the experimental data by using an improved empirical mode decomposition technique [12]. Similarly, Hong *et al.* decomposed the transient response signal into single-frequency modes using variational mode decomposition, and evaluated the damping properties by

The associate editor coordinating the review of this manuscript and approving it for publication was Arpan Kumar Pradhan.

identifying the decay pattern [13]. For transformers in power stations, it was found that the transient vibration acquired during the de-energizing process also contained structural information of the windings [8]. These results suggest the potential for diagnosing transformer windings by detecting the change of modal parameters.

An operating transformer's windings are affected by electromagnetic force, and their structural parameters should be different from those of static windings because of the nonlinear properties of insulations. For a normal winding, coil movement in the axial direction is restricted by the clamping device. On one hand, an operating winding is almost equivalent to a static winding when the clamping force is much larger than the electromagnetic force. On the other hand, the electromagnetic force will change the axial force distribution of the winding under a low clamping force. It is important to understand the dynamic characteristics of an on-load winding for transformer diagnosis. However, it is very dangerous to perform a free vibration test on a winding during operation. In this study, free vibration tests were conducted on a small-size winding model to explore the effects of electromagnetic force on modal parameters under a safety voltage.

The steady-state vibration of a power transformer can be regarded as a response subjected to harmonic excitation, which often has components at 100 Hz and its harmonic frequencies [14]. This is also the reason why it is difficult to extract the structure information from the vibration signals. Note that the transformers selected in this study are all working at 50 Hz grid frequency. The vibration at 100 Hz is commonly explained as the combined contribution from the magnetostrictive force and the electromagnetic force. The former is proportional to the quadratics of the magnetic flux in the core, while the latter is proportional to the square of the current in the windings. As the applied voltage is usually a suitably regulated sinusoidal signal at 50 Hz, the flux and current in idealized transformers are proportional to the input voltage. Because practical transformers have nonlinear hysteresis between the excitation current and the magnetic flux within the core, the magnetostrictive force also contains other harmonics of 100 Hz. Ji *et al.* presented the relationship between the 100 Hz component and the electrical parameters [15]. García *et al.* proposed an improved 100 Hz vibration model, which not only includes current and voltage, but also contains oil temperature and a power factor [16]. We found that the correlation between the 100 Hz vibration of different locations contains diagnostic information of the windings [17]. Recently, Zhang *et al.* investigated the applicability of operational modal analysis to extract the modal parameters of windings from operating transformers [18], however, the effectiveness of digital filters needs to be further verified.

The features and changes in the harmonic components of transformer vibration are necessary to identify possible changes in the mechanical properties of a transformer. Bartoletti *et al.* proposed a low-frequency parameter named the weighted total harmonic distortion to distinguish between normal and anomalous transformers [19]. Similarly, we proposed several signal-based parameters [20], including the frequency complexity analysis based on information entropy and vibration stationarity analysis based on a recurrence plot [21]. It was showed statistically that anomalous transformers have unpredictable high-frequency vibration components. Recently, advanced signal processing methods, such as empirical wavelet transform, have been used to discover the non-stationary components of the vibrations collected from anomalous transformers [22]. In this study, we focus on the relationship between the steady-state vibration response of windings and the load. During the process of transformer condition monitoring, the vibration and current signals usually appear in the form of time series. Therefore, a gated recurrent unit (GRU) neural network is adopted to explore the change in vibration amplitude with load for in-service transformers.

The outline of this paper is as follows. In Section II, the relationship between natural frequency change and load is investigated after the winding vibration model is introduced, and a GRU-based sequence model is developed by taking into account the effect of load current on harmonic response. Then, the frequency responses of a winding model under different clamping forces and loads are simulated in Section III. Laboratory experiments are carried out to verify the simulated results in Section IV. In Section V, the feasibility and efficiency of the proposed field application scheme are validated through analysis of typical in-service transformers. Finally, conclusions are drawn in Section VI.

II. THEORY

A. VIBRATION MODEL OF AN OPERATING WINDING

A typical winding structure of an oil-immersed high-voltage transformer is shown in Fig. 1. It comprises a stack of disk-type coils. The disks are composed of conductor strips insulated with kraft paper, and are separated by equally spaced pressboards. In the equivalent multi-degree-of-freedom (MDOF) model, m stands for the mass of each coil, and the insulation materials including pressboard and kraft paper are represented by a combination of stiffness (k) and damping (c). The above three parameters are considered to be the structural parameters in this study. In addition, f_i and x_i represent the electromagnetic force and displacement of the i-th coil, respectively. The whole winding unit is clamped between the top and bottom clamping beams. The motion of the bottom clamp is constrained, and the top clamp provides a constant axial clamping force.

Under the assumption that the core and frame are relatively stiff, the axial winding vibration model can be described:

$$\mathbf{M}\{\ddot{x}\} + \mathbf{C}\{\dot{x}\} + \mathbf{K}\{x\} = \{f\}, \tag{1}$$

where $\mathbf{M}$, $\mathbf{C}$, and $\mathbf{K}$ represent the mass, damping, and stiffness matrices, respectively, and $\{x\}$ and $\{f\}$ are the displacement and force vector, respectively. The induced electromagnetic force on each coil is proportional to the current squared,

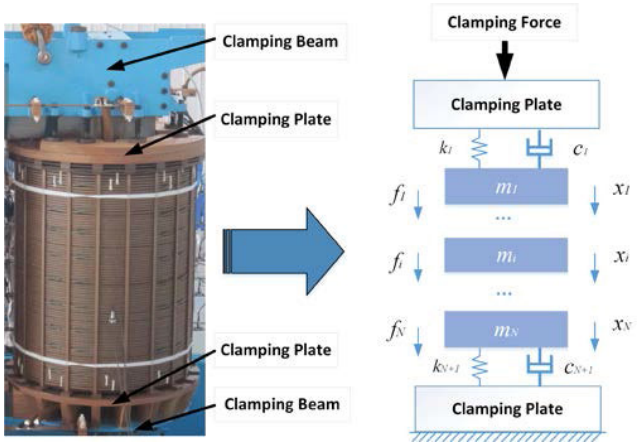

FIGURE 1. Simplified mathematical model of windings.

which can be denoted as:

$$f_i(t) = F_i[1 - \cos(2\omega t)], \quad F_i \propto I^2, \tag{2}$$

where I and ω are the rated value and frequency of the current. F_i is the force amplitude of the i-th coil, which can be obtained via static electromagnetic analysis. The function f_i consists of a DC part and an AC part, where the DC part changes the stress on the pressboard in the axial direction, while the AC part acts as an excitation force at frequency 2ω:

$$f_i = f_i^{DC} + f_i^{AC}, \tag{3}$$

The stiffness coefficient and stress-strain property of an insulation block are expressed respectively as [23]:

$$k = H\frac{d\sigma}{d\varepsilon} \text{ and } \sigma = \begin{cases} a\varepsilon + b\varepsilon^3 & (\varepsilon > 0) \\ 0 & (\varepsilon \le 0), \end{cases} \tag{4}$$

where σ and ε are stress and strain, respectively; a and b are material-related constants; and H is a constant related to the contact area and thickness of insulations. For a system with damping less than critical, the natural frequency of the n-th mode is denoted as:

$$\omega_n = \gamma_n\sqrt{k/m}, \tag{5}$$

where γ_n is a constant. Next, the derivative of ω_n with respect to σ is obtained as:

$$\frac{\Delta\omega_n}{\Delta\sigma} \approx \frac{d\omega_n}{d\sigma} = 3\gamma_n H^2 b\varepsilon k^{-3/2} m^{1/2}. \tag{6}$$

Here, a new parameter called the frequency shift rate (*FSR*) is defined as:

$$FSR(\omega_n) = \frac{\Delta\omega_n}{\omega_n} \approx \lambda \cdot \Delta\sigma, \lambda(\sigma) = 3H^2 b\varepsilon k^{-2} m, \tag{7}$$

where λ is a parameter related to the clamping force for a specified winding. Since the stress change is proportional to the change of the current squared, *FSR* is only dependent on the current change for the windings with the same clamping force:

$$FSR(\omega_n) \propto \Delta(I^2), \tag{8}$$

According to (4), the progressive loss of clamping force is reflected in the decrease of the equivalent stiffness. Therefore, the winding conditions can be assessed in terms of axial force distribution by evaluating the relationship between *FSR* and $\Delta(I^2)$.

B. LOAD-VARIED STEADY-STATE VIBRATION

The harmonic components other than 100 Hz can be regarded as the responses of the winding structure under the magnetostrictive force. Because the input voltage is approximately constant for an in-service transformer, the magnetostrictive force originating from the core can be treated as a stable harmonic excitation:

$$f^{core} = \sum_{\omega} F_{\omega}^{core} \sin\omega t, \tag{9}$$

where ω should be an integral multiple of the fundamental frequency (100 Hz). When the sinusoidal force at frequency ω is applied on each coil of the model shown in (1), the steady-state response in the physical coordinates under the assumption that there is a little damping [24] is:

$$x_q(\omega) = \sum_{n=1}^{N} \frac{\varphi_{qn} F_{\omega}^{core} \sum_j \varphi_{jn}}{\sum_j m_j \varphi_{jn}^2} \cdot \frac{\sin\omega t}{(\omega_n^2 - \omega^2)}, \tag{10}$$

where N is the total number of degrees-of-freedom, x_q is the displacement of the q-th coil, and φ_{jn} is the amplitude of the j-th degree of freedom in the n-th mode. Since all coils have the same mass for a winding, the following is satisfied when normal modes are used:

$$\sum_j m_j \varphi_{jn}^2 = 1. \tag{11}$$

It stands to reason that the maximum amplitude appears when the excitation frequency is close to a certain natural frequency. For a system with no closely spaced modes, it is assumed that the amplitude peak at frequency ω is only dominated by the nearest $n\prime$-th mode ($\omega \approx \omega_{n\prime}$), and the amplitude of the q-th coil in terms of acceleration is:

$$A_q(\omega) \approx \mu_{qn\prime} \frac{\omega^2}{(\omega^2 - \omega_{n\prime}^2)}, \mu_{qn\prime} = F_{\omega}^{core} \varphi_{qn\prime} \sum_j \varphi_{jn\prime}, \tag{12}$$

where $\mu_{qn\prime}$ is a constant coefficient related to the location, mode shape, and magnetostrictive force. Note that A_q may have a negative value. Next, the amplitude change due to the natural frequency change is obtained as:

$$\frac{\Delta A_q}{\Delta\omega_{n\prime}} \approx \frac{dA_q}{d\omega_{n\prime}} = \mu_{qn\prime} \frac{2\omega^2\omega_{n\prime}}{(\omega^2 - \omega_{n\prime}^2)^2}. \tag{13}$$

Based on (12) and (13), the *FSR* value of an operating winding can be estimated by:

$$FSR(\omega_{n\prime}) = \frac{\Delta\omega_{n\prime}}{\omega_{n\prime}} \approx \frac{\mu_{qn\prime}}{2} \frac{\Delta A_q(\omega)}{A_q^2(\omega)}. \tag{14}$$

Substituting (7) into (14), the relationship between the amplitude change and the stress change is:

$$\frac{\Delta A_q(\omega)}{A_q^2(\omega)} \approx \frac{2\lambda}{\mu_{qn'}}\Delta\sigma. \tag{15}$$

For an operating transformer, the vibration samples under different loads can be acquired, and a new parameter *SAC* is used to represent the sum of the amplitude change between any two samples:

$$SAC = \frac{1}{N_\omega}\sum_{\omega}\frac{\Delta A_q(\omega)}{A_q^2(\omega)} \propto \Delta(I^2), \tag{16}$$

where N_ω is the number of selected harmonic components. Compared with *FSR*, it is shown that *SAC* is also proportional to the change of current squared. However, the relationship between them not only reflects the winding clamping state, but also contains the information of the magnetostrictive force, mode shape, and sensor location. In field applications, *SAC* can be approximately used to assess the clamping state based on the following assumptions. First, f^{core} has a similar distribution function for all transformers. Second, the matrix $\mathbf{K}$ varies with the clamping force proportionately because the pressure on each pressboard changes synchronously, which results in unaffected mode shapes when the corresponding natural frequency changes, and it is assumed that all dominated modes are covered when enough harmonic peaks are taken into account. Third, the vibration sensors are arranged at the same or symmetrical locations on the tank during the measurement.

C. GRU-BASED MODEL IN FIELD APPLICATIONS

In field applications, six accelerometers are arranged on one side of the three-phase transformer tank, whose locations are illustrated in Fig. 2. The sensors in one column are related to one winding structure, whose positions are symmetrical with respect to the winding center. In addition, the sensor location should close to the winding end which is subjected to the largest axial electromagnetic force. The vibration and current signals are acquired synchronously at 10 kHz. Our measurement system records one second of data every minute, and the measurement continues for more than 24 hours to cover the entire load range.

The vibration acquired from the transformer tank is a mixed signal, and we focus on the harmonic components larger than 100 Hz. Based on the aforementioned theory, the vibration features of each location can be extracted by using the procedures shown in Fig. 3. The time point number T depends on the sampling interval. If the interval is set to one hour, then T is 24 for a one-day period. According to the requirement of (12), the absolute value of the selected peak should be larger than the threshold which is 0.2 times the root mean square of the vibration series. V_i and I_i represent the vibration series and current RMS at time index i, respectively. Note that I_i should be normalized by dividing its rated value first. According to (16), the *SAC* sequence is derived from the vibration sequence, and each element in the force change sequence $\{\Delta F_t\}$ equals to the change of the current squared.

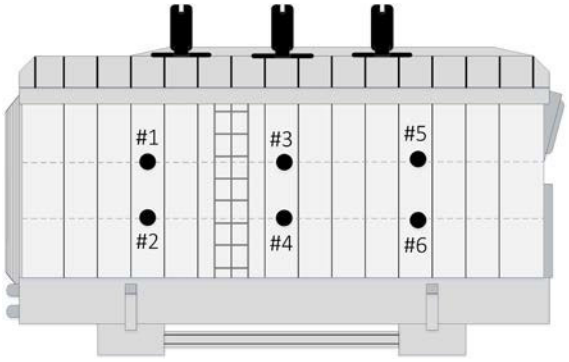

FIGURE 2. Sensor arrangement in the field applications.

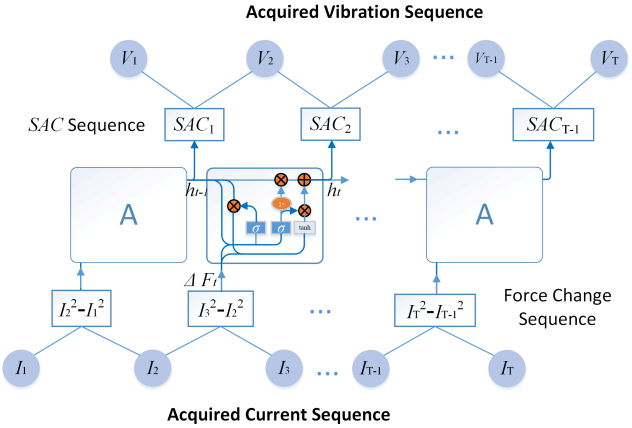

FIGURE 3. Flowchart of the GRU-based sequence model.

In this study, a GRU network is used to establish the relationship between *SAC* sequence and force sequence. According to (16), the GRU network is sufficient to interpret the linear relationship, which also has the ability to capture nonlinear patterns. In addition, the GRU network is a kind of improved recurrent neural networks, which aims to solve the vanishing gradient problem. The GRU cell is also illustrated in Fig. 3, and Eqs. (17)–(20) summarizes how to calculate the cell state:

$$z_t = Sigmoid(W_z \cdot [h_{t-1}, \Delta F_t]), \tag{17}$$
$$r_t = Sigmoid(W_r \cdot [h_{t-1}, \Delta F_t]), \tag{18}$$
$$h'_t = \tanh\left(W \cdot [r_t * h_{t-1}, \Delta F_t]\right), \tag{19}$$
$$h_t = z_t * h'_t + (1 - z_t) * h_{t-1}, \tag{20}$$

where r_t and z_t are reset gate and update gate, respectively. W, W_r and W_z are weight matrices. Because the load variation trend of each transformer is different, we introduce a method refers to the "learn and predict" procedure. First, the GRU network is trained by using the monitoring data. After that, the obtained GRU cell contains the sequence information. Then, the *SAC* sequence can be predicted by giving an arbitrary force sequence.

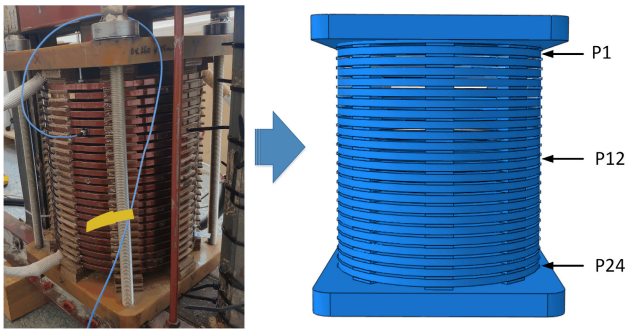

FIGURE 4. FE model based on the experimental winding.

TABLE 1. Specifications of the winding model.

Quantity	Value
Core diameter	113 mm
Height of LV and HV winding	264 mm and 264 mm
Inner and outer diameters of LV winding	126 mm and 166 mm
Inner and outer diameters of HV winding	186 mm and 230 mm
Rated current of LV and HV windings	40 A and 25 A
LV and HV winding turns	140 and 240
Disk number of LV and HV windings	24 and 24
Thickness and width of pressboards	3.5 mm and 40 mm

III. FINITE-ELEMENT SIMULATION

In this section, a finite-element (FE) model of the experimental winding structure is established using the software Abaqus. The 10 kVA single-phase winding and the corresponding FE model are illustrated in Fig. 4, and its parameters are given in Table 1. In the model, the degree of freedom of the bottom nodes is defined as zero because of the constraint boundary condition, and the pressure is applied on the top. The frequency response functions of each coil under different clamping forces are obtained in the simulation, and we focus on the effect of electromagnetic force on vibration responses.

The stress-strain property of the pressboard is obtained from compression and decompression measurements, which are depicted in Fig. 5. In the FE model, the hysteresis phenomenon is ignored, and the mean value is used instead. The electromagnetic force distribution can be obtained by establishing a 2-D axisymmetric model in ANSYS [9]. The axial electromagnetic force amplitude defined in (2) is obtained when the input current is 75 A, which is shown in Fig. 6. In order to make the results more visible, the input current is three times as large as the rated value. Because the maximum axial electromagnetic force always appears at the winding end, P1, P12, and P24 are selected as typical points.

A frequency response function (FRF) is a mathematical representation of the relationship between the input force and the measured vibration at a particular point. Note that the excitation force is applied to the top clamp in both simulation and experiment. For a clamping force (CF) of 2.4 MPa, the FRFs under different loads are compared in Fig. 7. Similarly, the FRFs under 0.2 MPa are compared

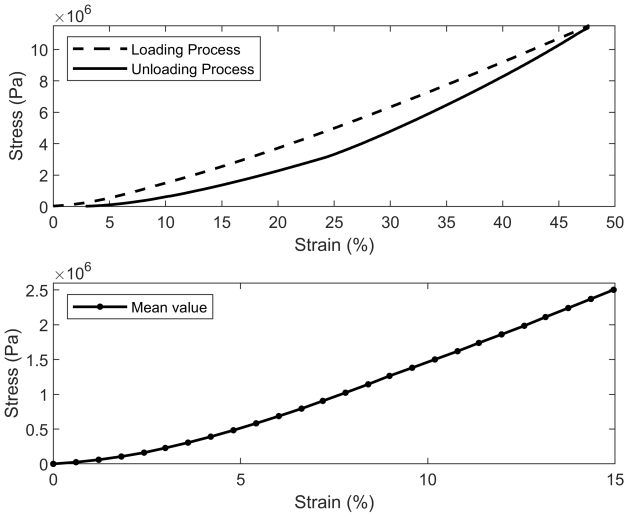

FIGURE 5. Stress–strain curves of the pressboard.

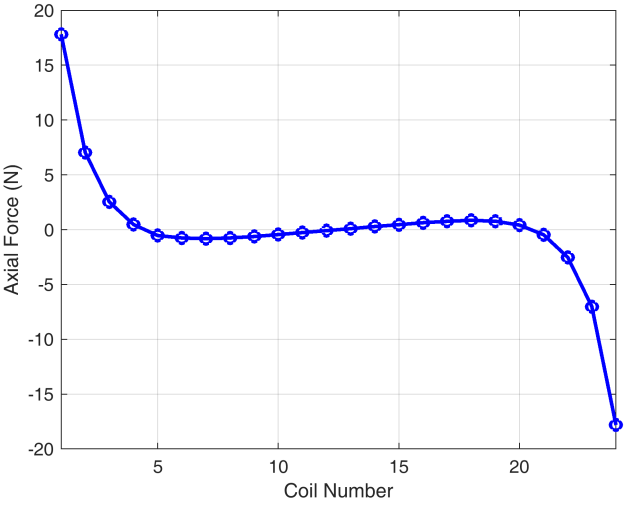

FIGURE 6. Electromagnetic force distribution at maximum current.

in Fig. 8. It can be seen that the electromagnetic force produced by the current is insufficient to change the structural parameters of the windings when the clamping force is large enough. By comparison, the electromagnetic force will cause the natural frequency of the structure to move to higher frequencies when the clamping force is 0.2 MPa. Similar movement patterns are observed in all the coils.

According to (7), *FSR* is only related to the stress change. Taking P1 as an example, the relationship between *FSR* and natural frequency is shown in Fig. 9, which is obtained by calculating the peak movement between the FRF curves under 0 A and 75 A. It is shown that the *FSR* value is independent of frequency, and the average *FSR* value is used instead in the remainder of this paper.

For P1, the relationship between *FSR* and current is plotted in Fig. 10. It can be seen that the *FSR* value is proportional to the current squared. According to (7), the slope of the line contains the structural information of the windings, which is also defined as $FSRR = FSR/I^2$. The *FSRR* values of three

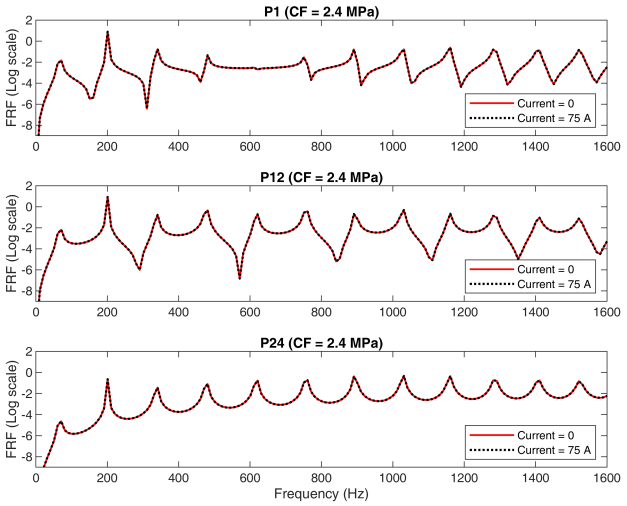

FIGURE 7. Comparison of FRF curves for the well-clamped windings.

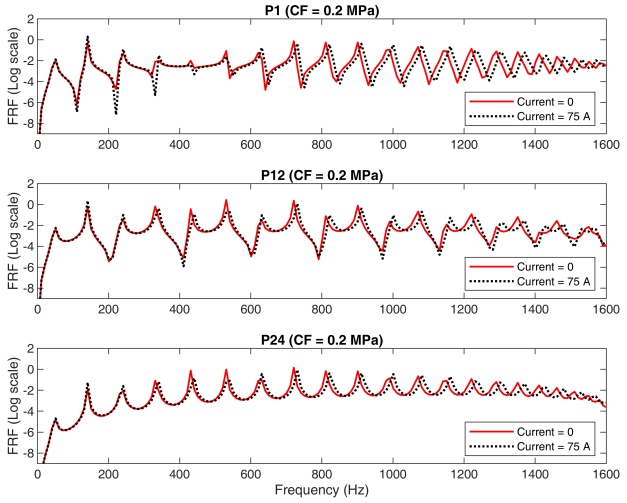

FIGURE 8. Comparison of FRF curves for the loose windings.

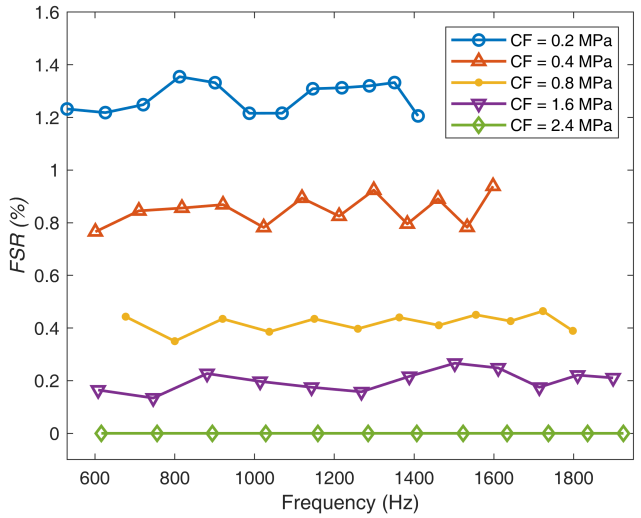

FIGURE 9. FSR values under different clamping forces.

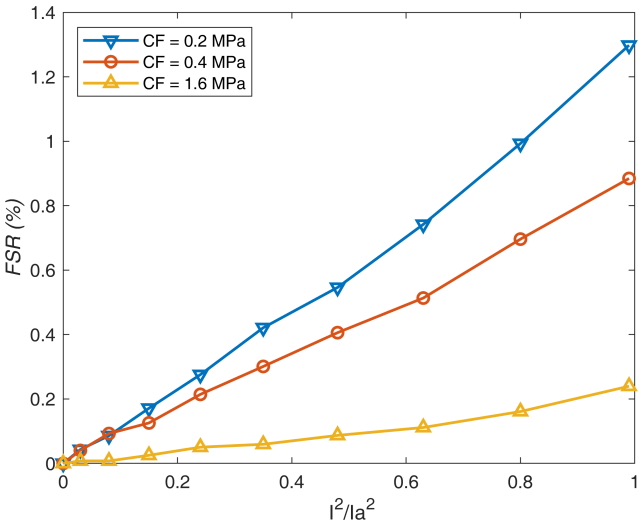

FIGURE 10. FSR as a function of current under different clamping forces.

typical points under different clamping forces are depicted in Fig. 11. It can be seen that all points have the same trend, so *FSRR* can be treated as a location-independent structural index.

IV. LABORATORY EXPERIMENT

During the laboratory experiment, free vibration tests were conducted on an on-load winding unit whose parameters are the same as those given in Table 1. The clamping force of the winding was adjusted by tightening the bolt to a specified torque, and the torque value was finally converted to the pressure on the pressboard. The accelerometers (Model 356A03) were glued on the coil, and the vibrations from P1, P12, and P24 were analyzed in detail. The integrated system B&K 3560C with PULSE software was used to acquire vibration data and calculate FRFs. During the experiment, the low-voltage terminals of the windings were short-circuited, and the high-voltage terminals were connected to the AC voltage regulator. Unlike in the FE simulation, the current was limited to the range of 0 to 25 A in the laboratory experiment. The current was increased gradually by adjusting the voltage. When the current reached the desired value, the transient vibration responses in the axial direction and related FRFs were obtained when the winding top was hit by an impact hammer (B&K 8206).

The FRF curves of three typical points under 2.0 MPa and 0.1 MPa are shown in Fig. 13 and Fig. 14, respectively. Due to the small size of the experimental windings, the effect of the load current on the low-frequency FRFs is not significant. When the clamping force is large enough, the load current hardly affects the natural frequency of the windings. By comparison, the peaks in the FRF curves shift to higher frequencies when the current increases for the loose windings. These results are consistent with the simulation results. Based on the FRFs, the natural frequencies of the system can be extracted by locating the peaks, which are compared in Table 2.

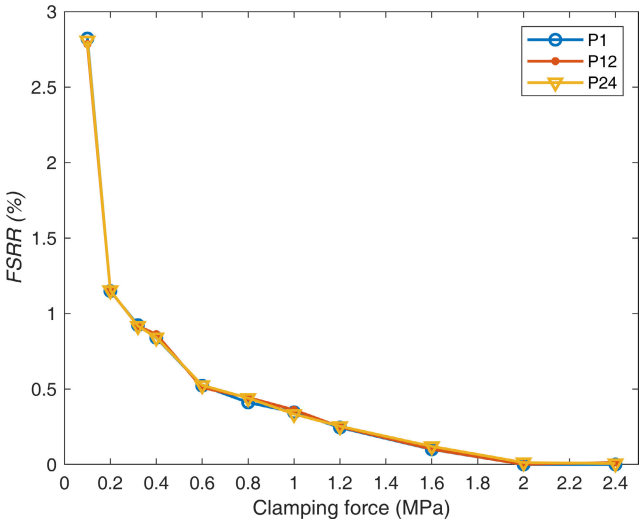

FIGURE 11. FSRR as a function of clamping force for selected points.

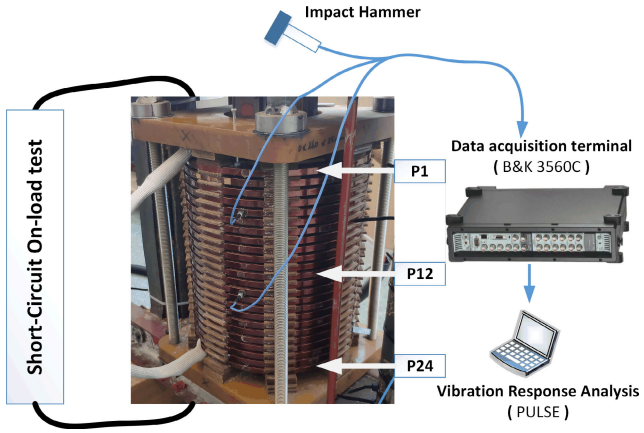

FIGURE 12. Single-phase model in the laboratory experiment.

TABLE 2. Comparison of the identified natural frequencies.

Natural frequency (Hz)					
CF = 2.0 MPa			CF = 0.1 MPa		
0A	25A	$\Delta\omega_n$	0A	25A	$\Delta\omega_n$
943	943	0	640	642	2
1197	1197	0	950	954	4
1331	1331	0	1130	1134	4
1518	1518	0	1344	1349	5
1830	1830	0	1485	1492	7
2218	2218	0	1671	1678	7
2610	2610	0	1886	1904	8

Based on the identified natural frequencies, the *FSRR* values are calculated by taking into account the peak movement and the current change. We still regard 75 A as a 100% value, which is consistent with the simulation results. Fig. 15 shows the *FSRR* values at different frequencies, and the averaged values under different clamping forces are also compared. The *FSRR* value increases rapidly with the decreasing clamping force when the clamping force is less than 0.5 MPa. Referring to the simulated curve shown in Fig. 11, the estimated

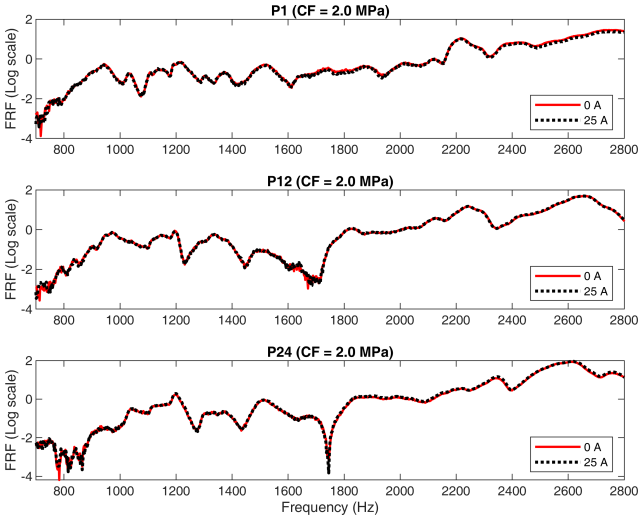

FIGURE 13. FRF curves under standard clamping force.

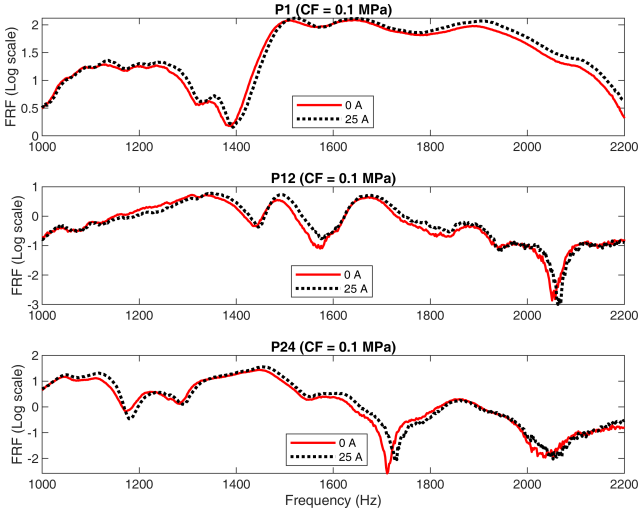

FIGURE 14. FRF curves under low clamping force.

clamping force can be derived from the *FSRR* value, which is close to the real value.

At the end of this section, we would like to discuss an interesting phenomenon. The pressboard at the top may lose contact with the coils when the clamping force drops to a low level. Because the direction of the electromagnetic force on the top coil is downward, the looseness becomes more severe when the current increases, and the quick reduction of the stiffness of pressboard will decrease the natural frequency. Fig. 16 shows that the FRF curve moves toward low frequency as the current increases when the clamping force is less than 0.1 MPa, which is opposite to the result shown in Fig. 14.

V. FIELD APPLICATIONS

According to [4], shrinkage and fading of the stiffness of solid insulation due to thermal degradation are the most common causes of the clamp looseness. So the clamping force adjustment experiment offers a reference for the study of the

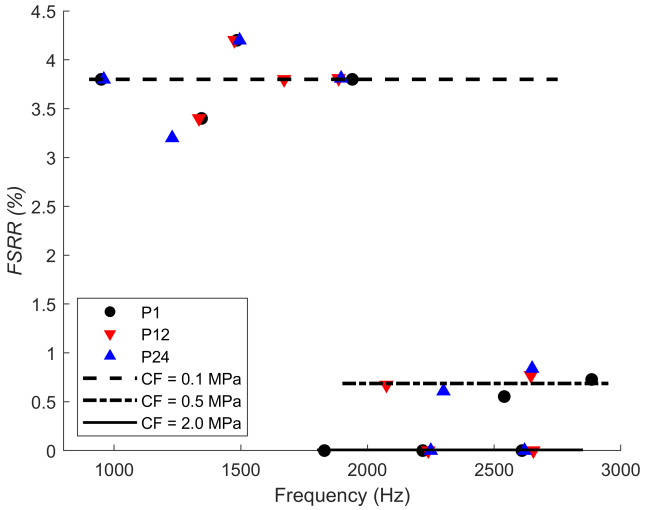

FIGURE 15. FSRR values at different frequencies.

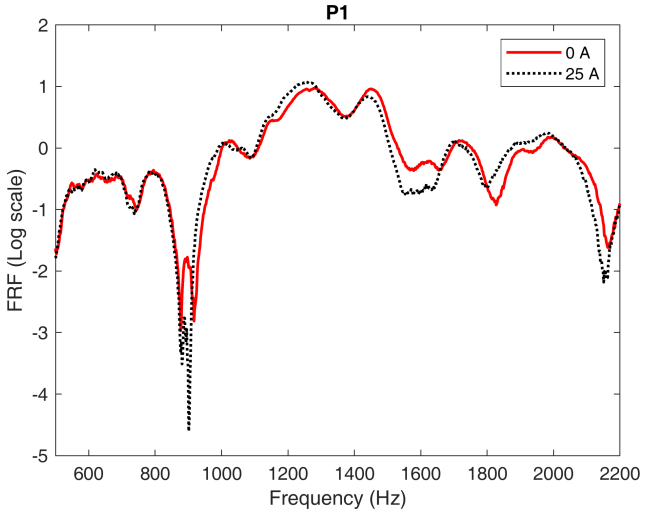

FIGURE 16. FRF curves for the loose contact windings.

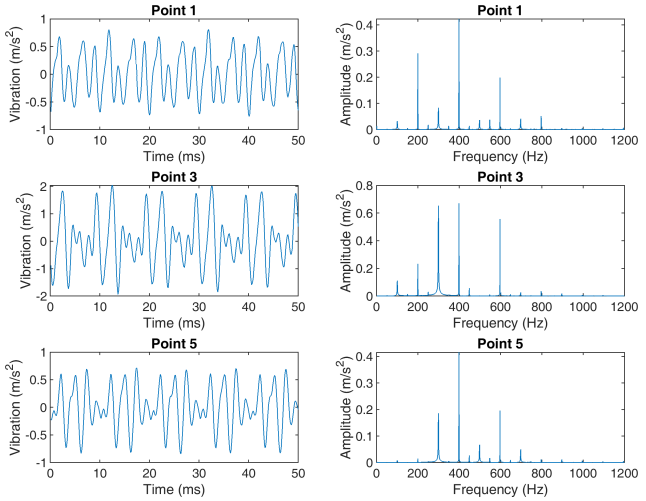

FIGURE 17. Vibrations of the normal transformer in the time and frequency domains.

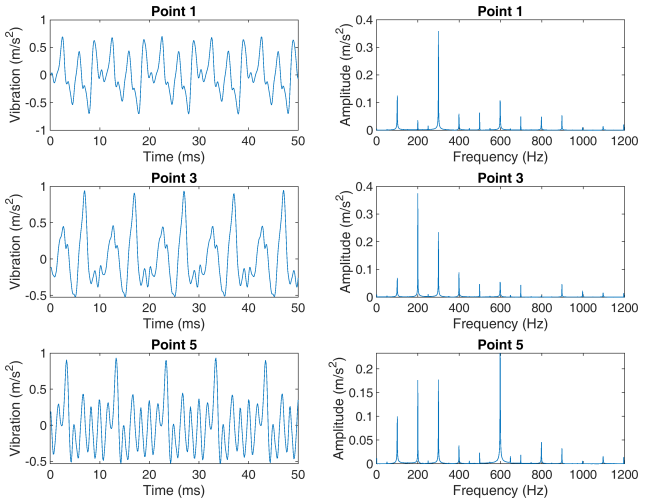

FIGURE 18. Vibrations of the degraded transformer in the time and frequency domains.

vibrations of degraded transformers. In this section, two typical transformers, including a normal sample and a degraded sample, are selected to demonstrate the applications of the proposed method. Both transformers have a primary voltage class of 110 kV, which means their winding structures are similar. The change in short-circuit impedance (SCI) between the measured value and the original (factory) value is used as the criterion to distinguish between normal transformer and degraded transformer. The normal sample has a change in SCI of below 0.5%, while the degraded sample is selected from the aged transformers with changes in SCI between 1% and 3% [2]. In this study, we did not choose the anomalous transformers for the reason that they cannot withstand high loads.

The vibrations were acquired from the transformers according to the procedure introduced in Section II. Typical vibrations from the normal transformer and the degraded transformer are shown in Fig. 17 and Fig. 18, respectively. Because the steady-state vibration has obvious periodicity, Fourier transform is sufficient for harmonic analysis. Point 1, Point 3, and Point 5 are located close to the winding top, and their vibrations in the time domain and frequency domain are both plotted in the figure. The amplitude and distribution of the harmonic components have the characteristics of randomness. So it is difficult to distinguish the degraded sample from the normal sample through the analysis of short-time vibrations.

Following the flowchart shown in Fig. 3, the *SAC* and force sequences can be obtained. Before the application of GRU networks, the scatter plots of the normal transformer are shown in Fig. 19. Note that the discrete points are obtained from the vibration monitoring data by adjusting the time interval. The red lines are obtained using the least-squares method, and should pass through the origin point. The drawback of the traditional linear regression method is that a large number of points are needed to obtain better fitting results. In addition, the nonlinear information will be lost if the linear regression is used.

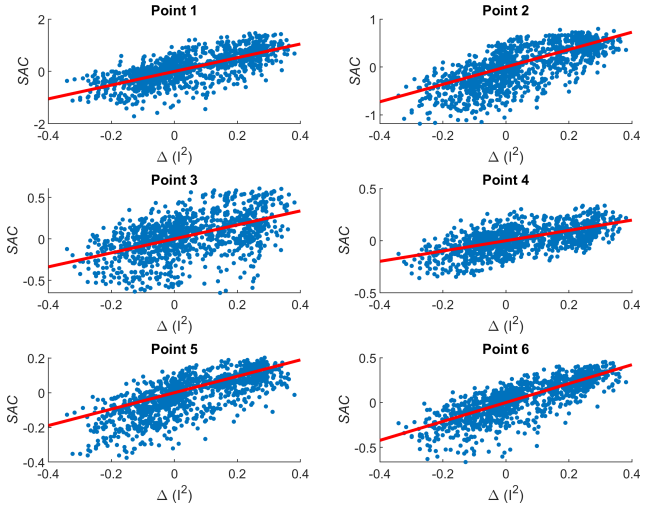

FIGURE 19. Relationship between SAC and force sequences for the normal transformer.

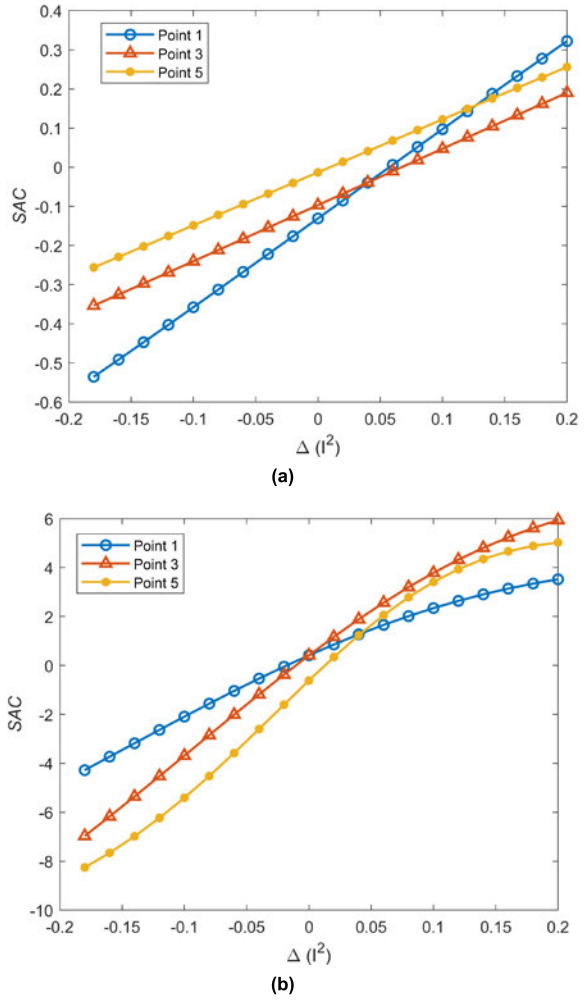

FIGURE 20. Predicted SAC curves for the typical transformers: (a) normal sample, (b) degraded sample.

Finally, the proposed ''learn and predict'' procedure is applied to the selected typical transformers, and the predicted relationship between *SAC* sequence and force sequence is shown in Fig. 20. The GRU network is realized by using gruLayer in MATLAB. In this study, the time interval of the sequence is one hour, and the single-element force sequence from -0.2 to 0.2 is used to predict the *SAC* values after the GRU network is trained by the monitoring data. Compared with the fitted lines in Fig. 19, it is proved that the GRU network can capture the linear relationship accurately. In Fig. 20, the curve slope for the degraded transformer is larger than that for the normal transformer. According to (15), the curve slope reflects the clamping force on the pressboard, which can be used as a health index for winding condition assessment.

VI. CONCLUSION

Research on the effect of load current on the vibration response of windings is of great importance for the diagnosis of in-service transformers. Based on the nonlinear stress–strain property of the insulations, the frequency responses of a single-phase winding under different loads were simulated. The electromagnetic force produced by the load current is insufficient to change the structural parameters of well-clamped windings. In contrast, an increased current will cause the natural frequency of the windings to move to higher frequencies when the clamping force is low. In the laboratory experiment, free vibration tests were conducted on an on-load winding structure, and the results agreed with those obtained in the finite-element simulation. The ratio of natural frequency change to current squared was found to be a good indicator of clamping force. In the field applications, the GRU-based ''learn and predict'' procedure is proposed, which can be used to capture the relationship between the vibration change and the corresponding current change. It was shown that the change of harmonic amplitude with load current contains the structural information of windings, which can be used to distinguish normal transformers from degraded transformers. In summary, transformer condition monitoring using vibration methods should not be limited to analyzing a single time vibration segment, but should also grasp the diagnostic information from the load-varying vibration trend.

REFERENCES

[1] M. M. Islam, G. Lee, and S. N. Hettiwatte, ''A review of condition monitoring techniques and diagnostic tests for lifetime estimation of power transformers,'' *Electr. Eng.*, vol. 100, no. 2, pp. 581–605, Jun. 2018.

[2] M. Bagheri, M. Naderi, T. Blackburn, and T. Phung, ''Frequency response analysis and short-circuit impedance measurement in detection of winding deformation within power transformers,'' *IEEE Elect. Insul. Mag.*, vol. 29, no. 3, pp. 33–40, May 2013.

[3] D. Martin, J. Marks, and T. Saha, ''Survey of Australian power transformer failures and retirements,'' *IEEE Elect. Insul. Mag.*, vol. 33, no. 5, pp. 16–22, Sep. 2017.

[4] L. Naranpanawe, C. Ekanayake, T. K. Saha, and P. K. Annamalai, ''Influence of moisture dependency of pressboard on transformer winding clamping pressure,'' *IEEE Trans. Dielectr. Electr. Insul.*, vol. 24, no. 5, pp. 3191–3200, Oct. 2017.

[5] M. Bagheri, M. S. Naderi, and T. Blackburn, ''Advanced transformer winding deformation diagnosis: Moving from off-line to on-line,'' *IEEE Trans. Dielectr. Electr. Insul.*, vol. 19, no. 6, pp. 1860–1870, Dec. 2012.

[6] Y. Konishi, M. Kato, M. Hasegawa, H. Aoyama, M. Onuki, and S. Matsumoto, "Tank vibration analysis of an extra-high-voltage transformer," *IEEJ Trans. Electr. Electron. Eng.*, vol. 15, no. 5, pp. 781–788, May 2020.
[7] Y. Wang and J. Pan, "Comparison of mechanically and electrically excited vibration frequency responses of a small distribution transformer," *IEEE Trans. Power Del.*, vol. 32, no. 3, pp. 1173–1180, Jun. 2017.
[8] K. Hong, X. Huang, and S. Xu, "A study of nonlinear behavior of transformer windings in structural degradation detection," *J. Vibrat. Acoust.*, vol. 142, no. 1, pp. 1–9, Feb. 2020.
[9] A. Secic, M. Krpan, and I. Kuzle, "Vibro-acoustic methods in the condition assessment of power transformers: A survey," *IEEE Access*, vol. 7, pp. 83915–83931, Jul. 2019.
[10] D. O. Swihart and D. V. Wright, "Dynamic stiffness and damping of transformer pressboard during axial short circuit vibration," *IEEE Trans. Power App. Syst.*, vol. PAS-95, no. 2, pp. 721–730, Mar. 1976.
[11] H. Zhang, B. Yang, W. Xu, S. Wang, G. Wang, Y. Huangfu, and J. Zhang, "Dynamic deformation analysis of power transformer windings in short-circuit fault by FEM," *IEEE Trans. Appl. Supercond.*, vol. 24, no. 3, pp. 1–4, Jun. 2014.
[12] C. Geng, F. Wang, J. Zhang, and Z. Jin, "Modal parameters identification of power transformer winding based on improved empirical mode decomposition method," *Electr. Power Syst. Res.*, vol. 108, pp. 331–339, Mar. 2014.
[13] K. Hong, L. Wang, and S. Xu, "A variational mode decomposition approach for degradation assessment of power transformer windings," *IEEE Trans. Instrum. Meas.*, vol. 68, no. 4, pp. 1221–1229, Apr. 2019.
[14] M. Bagheri, A. Zollanvari, and S. Nezhivenko, "Transformer fault condition prognosis using vibration signals over cloud environment," *IEEE Access*, vol. 6, pp. 9862–9874, Mar. 2018.
[15] J. Shengchang, L. Yongfen, and L. Yanming, "Research on extraction technique of transformer core fundamental frequency vibration based on OLCM," *IEEE Trans. Power Del.*, vol. 21, no. 4, pp. 1981–1988, Oct. 2006.
[16] B. Garcia, J. C. Burgos, and A. M. Alonso, "Transformer tank vibration modeling as a method of detecting winding deformations—Part II: Experimental verification," *IEEE Trans. Power Del.*, vol. 21, no. 1, pp. 164–169, Jan. 2006.
[17] K. Hong, H. Huang, and J. Zhou, "Winding condition assessment of power transformers based on vibration correlation," *IEEE Trans. Power Del.*, vol. 30, no. 4, pp. 1735–1742, Aug. 2015.
[18] F. Zhang, S. Ji, H. Ma, and T. K. Saha, "Operational modal analysis of transformer windings," *IEEE Trans. Power Del.*, vol. 35, no. 3, pp. 1285–1298, Jun. 2020.
[19] C. Bartoletti, M. Desiderio, D. DiCarlo, G. Fazio, F. Muzi, G. Sacerdoti, and F. Salvatori, "Vibro-acoustic techniques to diagnose power transformers," *IEEE Trans. Power Del.*, vol. 19, no. 1, pp. 221–229, Jan. 2004.
[20] K. Hong, H. Huang, J. Zhou, Y. Shen, and Y. Li, "A method of real-time fault diagnosis for power transformers based on vibration analysis," *Meas. Sci. Technol.*, vol. 26, no. 11, Nov. 2015, Art. no. 115011.
[21] N. Marwan, M. Carmenromano, M. Thiel, and J. Kurths, "Recurrence plots for the analysis of complex systems," *Phys. Rep.*, vol. 438, nos. 5–6, pp. 237–329, Jan. 2007.
[22] M. Zhao and G. Xu, "Feature extraction of power transformer vibration signals based on empirical wavelet transform and multiscale entropy," *IET Sci., Meas. Technol.*, vol. 12, no. 1, pp. 63–71, Jan. 2018.
[23] M. Patel, "Dynamic response of power transformers under axial short circuit forces part II–windings and clamps as a combined system," *IEEE Trans. Power App. Syst.*, vols. PAS–92, no. 5, pp. 1567–1576, Sep. 1973.
[24] R. E. Blake, "Basic vibration theory," in *Harris' Shock and Vibration Handbook*, 5th ed. New York, NY, USA: McGraw-Hill, 2002.

KAIXING HONG was born in Zhejiang, China, in 1985. He received the B.S. degree in mechanical engineering and the Ph.D. degree in instrumentation science and engineering from Zhejiang University, Hangzhou, China, in 2007 and 2016, respectively.

He is currently an Associate Professor with China Jiliang University. His research interests include signal processing algorithm, machine learning, and power transformer fault diagnosis.

JIE PAN (Member, IEEE) was born in Nanjing, China, in 1957. He received the B.Sc. degree from the Department of Physics, Nanjing University, China, and the Ph.D. degree from the Department of Mechanical Engineering, Adelaide University, Australia.

He is currently a Winthrop Professor with The University of Western Australia. His research interests include acoustics, vibration, control, and vibration-based condition monitoring of power transformers and water pumps. He is also a member of the Acoustical Society of America and a Fellow of the International Society of Engineering Asset Management.

MING JIN was born in Nanjing, China, in 1982. He received the B.E. degree in electrical communication engineering from Nanjing Normal University, China, in 2004, and the M.Sc. and Ph.D. degrees in mechanical engineering from The University of Western Australia, in 2009 and 2015, respectively.

He is currently a Research Assistant with the School of Mechanical and Chemical Engineering, The University of Western Australia. His research interests include vibration-based condition monitoring methods for high-power rating transformers, fundamental study of the vibration characteristics of windings, and diagnosis models of power transformers.